IEEE Access
Multidisciplinary | Rapid Review | Open Access Journal

Received November 9, 2021, accepted December 21, 2021, date of publication December 30, 2021,
date of current version January 11, 2022.

Digital Object Identifier 10.1109/ACCESS.2021.3139733

Terrain Simplification Algorithm in Radio Wave Propagation Prediction

DAN SHI, (Member, IEEE), ZHEN ZHANG, FENGSHUO WEI, AND CHENG LIAN
School of Electronic Engineering, Beijing University of Post and Telecommunications, Beijing 100876, China

Corresponding author: Dan Shi (shidan@buptemc.com)

This work was supported by the National Natural Science Foundation of China under Grant 61771069.

ABSTRACT Due to the diversity of landforms, an appropriate threshold should be selected for the simplification of different landforms. The distribution of simplified index was obtained by preprocessing the terrain data, and the distribution was used as a reference for threshold selection. In order to study the influence of terrain simplification on the prediction of complex electromagnetic environment, a visibility algorithm used in the regular model of terrain and a probability-based power propagation model are proposed. The visibility algorithm used in the regular model of terrain is based on the relationship between planes and triangular planes in three-dimensional space. The visible triangular surfaces and the corresponding visible area of the triangular surfaces in the terrain can be calculated with the visibility algorithm. The probability-based power propagation model uses the results of the visibility algorithm to calculate the propagation probability and calculates the change of receiver power in combination with the radio wave propagation characteristics. The spatial visibility algorithm and the probability-based power propagation model can be applied to the complex electromagnetic environment to analyze the influence of terrain simplification on prediction accuracy. The minimum error between the simulation result of the probability-based power propagation model and the Wireless InSite simulation result is 0.5018dB, and the average error is 1.5039dB.

INDEX TERMS Terrain simplification, spatial visibility, probability-based model.

I. INTRODUCTION

Digital Elevation Model (DEM) [1] describes the fluctuation of terrain through the elevation value of terrain, which is the basic element of the radio wave propagation prediction model [2]. However, the large number of triangular surfaces needed to divide the original terrain is a major factor affecting the computational efficiency of the radio wave propagation prediction model [3]–[7] based on the ray-tracing method. There are three ways to improve the simulation speed of ray-tracing algorithm: reducing the number of useless intersecting calculations [8]; improving the speed of intersecting calculation [8]; reducing the grids in dividing terrain [9]. In this paper, terrain data is compressed to reduce the number of triangular surfaces needed for dividing terrain. The prediction results of the model will be affected when the simplified terrain is applied to the complex electromagnetic environment model. To analyze the influence from the perspective of terrain change, this paper proposes a visibility algorithm based on the relationship between planes and triangular planes in three-dimensional space and a probability-based power propagation model.

Researchers carried out lots of related methods in the aspect of terrain simplification. Vertex coordinate was expressed in the form of a two-dimensional matrix with wavelet analysis [10], [11]. Wavelet decomposition and reconstruction algorithm [12], [13] was used to decompose the matrix into lots of low-frequency domain information and high-frequency domain information and the signals of different frequencies are synthesized. However, the parameters of wavelet analysis have no direct correlation with terrain features, which influence the reconstruction effect of DEM greatly. Douglas–Peucker (DP) algorithm [14], [15] was widely used in line element simplification. The three-dimensional DP uses the distance from the point to the base plane as the basis for choosing the value of each discrete point [16], but it is inefficient. In this paper, vertex coordinate is expressed in the form of a two-dimensional matrix. The matrix is divided into blocks in 3×3 size. The DP operation in the four directions of the row, column, negative and positive diagonal of each block is considered comprehensively.

The associate editor coordinating the review of this manuscript and approving it for publication was Zhengqing Yun.

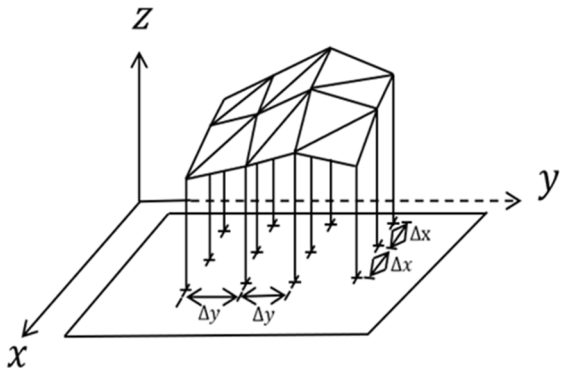

FIGURE 1. The regular model of the terrain.

From the perspective of power propagation, it is necessary to ensure that the triangular surface is visible for the next. The painter's algorithm [17] raster-scans the object from far to near relative to the observation screen to judge the visibility problem between objects. It is applicable when there is no intersection or cyclic overlap between polygons [18]. The depth cache algorithm [19]–[21] uses the depth cache of each pixel to safeguard occlusion information. In addition, [22]–[27] find the two-dimensional or three-dimensional surface visible to the transmitter through computer graphics algorithm. However, the algorithms mentioned above study the visible surface of the transmitter, which can be regarded as a point in the scene rather than a plane. They cannot specifically obtain the area of the visible parts of the observed triangular surfaces. To solve this problem, a visibility algorithm used in the regular model of the terrain is proposed is this paper. By defining the reference point, dividing line, the set of points, and studying the relationship between space planes and triangular planes in three-dimensional space, the visible surfaces and their visible areas can be calculated with the visibility algorithm.

The rest of this paper is structured as follows. The simplification method of regular terrain triangular mesh model is introduced in Section II. A visibility algorithm based on the relationship between triangular surface and space plane in three-dimensional space is proposed in Section III, which can eliminate terrain triangular surfaces that are not visible by the observation point and calculate the area of terrain triangular surfaces visible by the observation point. The ''calculation of the set of the visible surfaces'' of the algorithm can be used to derive the probability-based power propagation model in Section IV, which is used to analyze the influence of terrain simplification on electromagnetic prediction accuracy. By comparing and analyzing the simulation results of the probability-based power propagation model with the simulation results of Wireless Insite, the accuracy of the model proposed in this paper is verified in Section V, followed by the conclusion in Section VI.

II. TERRAIN SIMPLIFICATION

The regular model of the terrain, as shown in Fig. 1, is equally divided at spacings of Δx and Δy in the x and y directions

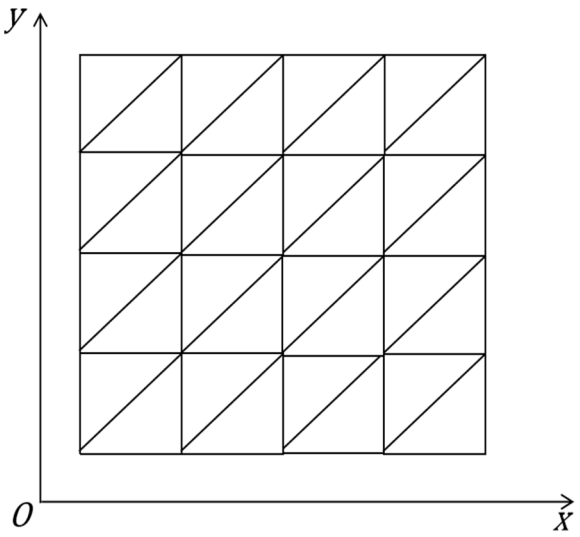

FIGURE 2. The top view of the regular terrain.

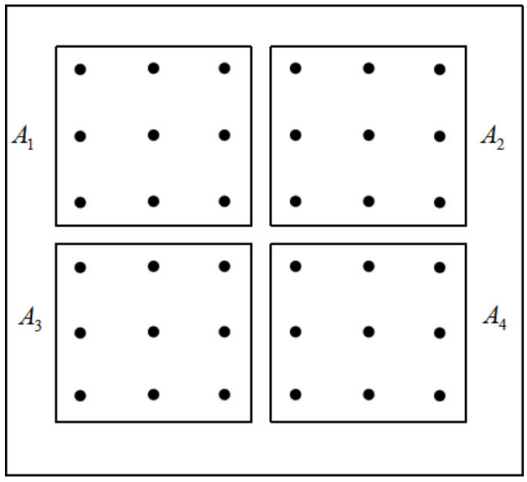

FIGURE 3. A large terrain is divided into four terrain blocks.

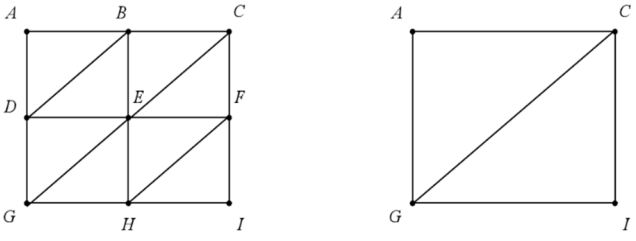

FIGURE 4. Simplified terrain blocks in 3 × 3 size.

respectively. The top view of the regular terrain is shown in Fig. 2.

DP algorithm judges whether to keep the point or not according to the relationship between the threshold and the vertical distance from the point to the line. The method of applying the DP algorithm to terrain simplification in this paper is: the height data of terrain is expressed in the form of two- dimensional numerical matrix, then the matrix is

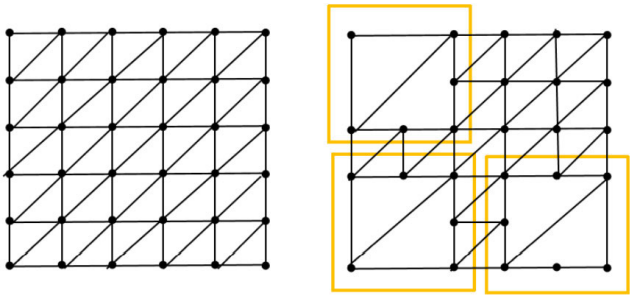

FIGURE 5. The terrain without simplification and the terrain with simplification.

divided into 3 points ×3 points as a terrain block. As shown in Fig. 3, a large terrain is divided into four terrain blocks: $A1$, $A2$, $A3$ and $A4$. This processing method will reserve some points in advance and avoid the narrow triangular surface after simplification, so this method will not cause a large difference between the simplified terrain and the real terrain.

The advantage of using terrain blocks to process the terrain is that it can eliminate the disadvantage of lacking the influence of adjacent nodes in a certain direction when using DP algorithm to simplify the terrain. Therefore, for the terrain block shown in the Fig. 4, this paper uses the DP operation in the four directions of row, column, positive and negative diagonal to determine whether the point E is retained or deleted. The point sets in four directions are {B, E, H}, {D, E, f}, {A, E, I} and {C, E, G}. Then each point set has a vertical distance value about point E, and the maximum value is taken as the vertical distance of point E. In this way, each terrain block will get a vertical distance value. The statistical vertical distance distribution is used as a reference for selecting terrain simplification threshold. Fig. 5 shows the terrain without simplification and the terrain with simplification.

This method saves the vertical distance of each terrain block to directly compare the vertical distance of each terrain block with the threshold to judge whether this terrain block should be simplified or not. Since the second DP operation is not required.

III. VISIBILITY ALGORITHM BASED ON TRIGONOMETRIC PLANES AND SPATIAL PLANES RELATIONSHIP

In the complex electromagnetic environment, some rays transmitted by the transmitter are propagated to the free space, and others are received by the receiver through the transmission between the surfaces. The transfer of power from one surface to the next involves the judgment of visibility. This paper puts forward a visibility algorithm based on the relationship between the triangular plane and plane in three-dimensional space to calculate the visible surfaces and the corresponding visible area in the regular model of the terrain. These results are applied to the probability-based power propagation model.

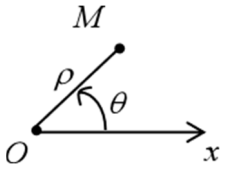

FIGURE 6. Polar system.

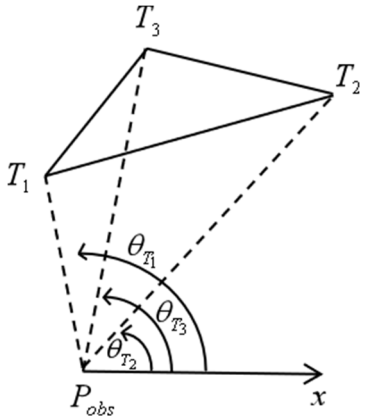

FIGURE 7. The relationship between the observation point and triangular surface.

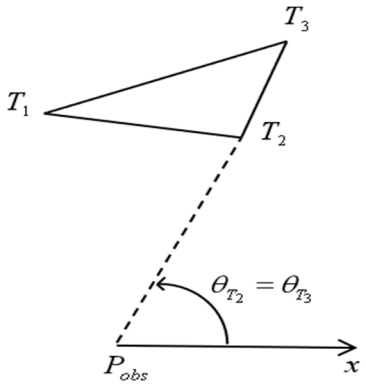

FIGURE 8. The polar angle of two vertices in triangular surface is equal.

A. DEFINITION OF REFERENCE POINT AND DIVIDING LINE

In Fig. 6, the pole of polar system is represented by O and the axis of polar system is represented by Ox. The coordinate of any point M in the polar system is (ρ, θ), in which ρ is the distance between points M and O. This distance is called the polar diameter and θ is the angle between vector $\overrightarrow{OM}$ and the polar axis, which is called the polar angle.

In three-dimensional space, there is a triangular surface $\Delta T_1T_2T_3$ out of the observation point p_{obs}. Two requirements need to be met for the observed triangular surface to be visible to the observation point. The normal vector of the observed triangular surface is $\overrightarrow{n_{b\_c}}$. Any point of the observed triangular surface is p. If the observed triangular surface can be seen by the observation point, no other object completely blocks the observation point and the observed triangular surface, and at least one group of (p_{obs}, p) satisfies the following formula

$$\theta < \overrightarrow{pp_{obs}}, \overrightarrow{n_{b\_c}} > \in \left[0, \frac{\pi}{2}\right) \qquad (3-1)$$

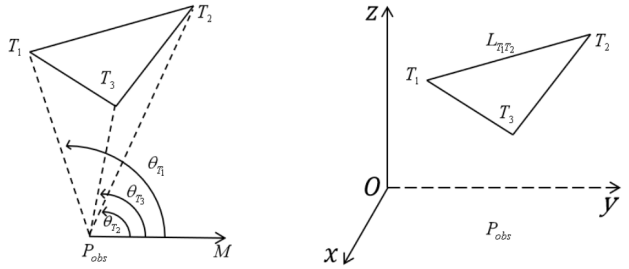

FIGURE 9. The reference point $T3$ and the dividing line L_{T1T2}.

The angle between the vector $\overrightarrow{pp_{obs}}$ from any point of the observed triangular surface to the observation point and the normal vector of the observed triangular surface is within the interval $[0, \pi/2)$.

As is shown in Fig. 7, the observation point is taken as the pole and the $p_{obs}x$ as the polar axis. The corresponding polar angle of the three vertices T_1, T_2 and T_3 are θ_{T1}, θ_{T2} and θ_{T_3} ($\theta_{T_1} > \theta_{T_3} > \theta_{T_2}$). The vertex with the second largest polar angle in the observed triangular surface will be used as the reference point. In Fig. 7, T_3 is used as the reference point. If the polar angle of the two vertices in the observed triangular surface is equal, the vertex far from the observation point will be selected as the reference point. As shown in Fig. 8, T_3 is selected as the reference point in the observed triangle surface.

A straight line is constructed of two points in the observed triangular surface except the reference point, which is called the dividing line. In Fig. 7 and Fig. 8, vertex T_3 is the reference point. Except for the reference point T_3, the two vertices T_1 and T_2 form the dividing line L_{T1T2}. The reference point T_3 and the observation point p_{obs} are on both sides of the dividing line. In Fig. 9, vertex T_3 is the reference point. Except for the reference point T_3, the two vertices T_1 and T_2 form the dividing line L_{T1T2}. The reference point T_3 and the observation point p_{obs} are on the same side of the dividing line.

B. DEFINITION OF THE SET OF POINTS

A dictionary represented by a symbol map is defined in this paper. The key of dictionary is polar angle intervals and the value is the space plane, which is formed by two vertices of a terrain triangular surface and the observation point. The elements in the dictionary are ordered from the smallest to the largest in accordance with the key. The values of the adjacent elements in the dictionary are on the common edges, namely, the adjacent space planes have common edges.

The dictionary of the observation point p_{obs} is represented by the symbol map_{obs}. In the polar system with the observation point as the pole, the polar angle interval of the observed triangular surface out of the pole can be obtained in the polar system. In Fig. 7, the polar angle interval of the observed triangular surface is $[\theta_{T_2}, \theta_{T_1})$. The set of all space planes in map_{obs} containing the polar angle range of the observed triangular plane is denoted as $\{\Pi\}$. The set of points formed

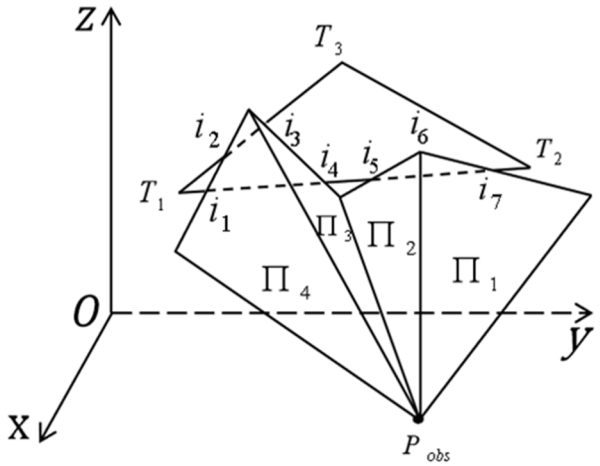

FIGURE 10. Model of spatial plane occluding triangular surface.

by the intersection of the two adjacent space planes in $\{\Pi\}$ and the plane of the observed triangular surface inside the observed triangular surface is denoted as Φ_{inner}. The set of points formed by the intersection of the two adjacent space planes in $\{\Pi\}$ and the edges of the observed triangular surface is denoted as Φ_{bd}. If the edges of the triangular surface overlap with the plane in $\{\Pi\}$, then the intersection point is the point at the two ends of the overlapping line segments. Then we define a set Φ_1, which is the union of Φ_{bd} and Φ_{inner}. In the free space, if a point is located above the plane, the point is visible from the observation point, which is called the visible point. It is not visible if the point is below the plane. The case of separate occlusion between the point and the observation point is not discussed here. If the vertex of the triangular surface is in the plane of $\{\Pi\}$, it is the intersection point. The set of visible vertices in the observed triangular surface is represented by Φ_2, and the set of invisible vertices is represented by Φ_3. The reference point is not involved in Φ_1, Φ_2 and Φ_3.

C. CALCULATION OF THE AREA OF THE VISIBLE SURFACE

According to the fact that whether the observation point and the reference point are on the same side of the dividing line and the relationship between the reference point and the space plane, the area of the triangular surface that can be seen by the observation point is calculated in six cases:

Case one: The observation point and the reference point are on the different sides of the dividing line. The reference point is located above the space plane.

The area of the observed triangular surface that can be seen from the observation point is

$$S = \left| \sum_{p_m, p_n \in \Phi_y} \lambda_{p_m, p_n} S_{\Delta p_m p_n p_s} \right| \qquad (3-2)$$

where, $\Phi_y = \Phi_1 + \Phi_2$. The elements in Φ_y are deduplicated and arranged in descending polar order. p_m and p_n are adjacent points in Φ_y. p_s is the reference point. λ is

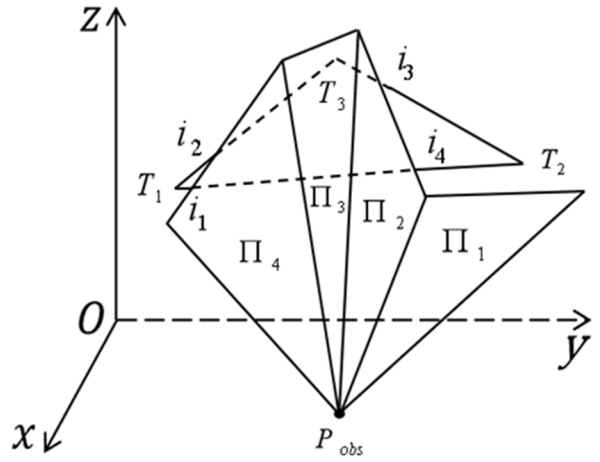

FIGURE 11. Model of spatial plane occluding triangular surface.

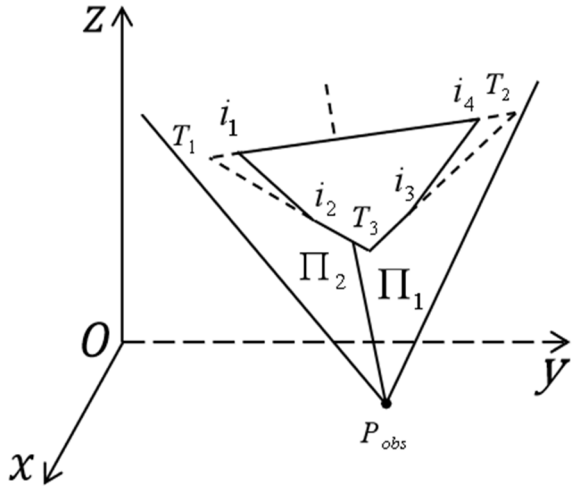

FIGURE 12. Model of spatial plane occluding triangular surface.

expressed as

$$\lambda_{p_m,p_n} = \begin{cases} 1 & \alpha_{p_m} < \alpha_{p_n} \\ 0 & \alpha_{p_m} = \alpha_{p_n} \\ -1 & \alpha_{p_m} > \alpha_{p_n} \end{cases} \quad (3-3)$$

$$\alpha = \arccos\left(\frac{\overrightarrow{p_s p} \cdot \overrightarrow{p_s T}}{\left|\overrightarrow{p_s p}\right| \cdot \left|\overrightarrow{p_s T}\right|}\right) \quad (3-4)$$

where, p_s is the reference point. T is any vertex in the observed triangular surface except the reference point.

As shown in Fig. 10, p_s is equal to T_3, which is above the space plane. $\{\Pi\} = \{\Pi_1, \Pi_2, \Pi_3, \Pi_4\}$. i_6 is the intersection point of the two adjacent space planes in $\{\Pi\}$ and the plane of $\Delta T_1T_2T_3$. i_1, i_2, i_3, i_4, i_5, i_7 are the intersection points of the space plane in $\{\Pi\}$ and the edge of $\Delta T_1T_2T_3$. $\Phi_1 = \{i_1, i_2, i_3, i_4, i_5, i_6, i_7\}$, $\Phi_2 = \{T_1, T_2\}$.

Case two: The observation point and the reference point are on the different sides of the dividing line, and the reference point is located below the space plane.

The area of the observed triangular surface that can be seen from the observation point is

$$S = \left|\sum_{p_m,p_n\in\Phi_{r,y}} \lambda_{p_m,p_n} S_{\Delta p_m p_n p_s}\right| + \left|\sum_{p_m,p_n\in\Phi_{l,y}} \lambda_{p_m,p_n} S_{\Delta p_m p_n p_s}\right| \quad (3-5)$$

where, $\Phi_y = \Phi_1 + \Phi_2$. The elements in Φ_y are deduplicated and arranged in descending polar order. $\Phi_{l,y}$ is the set of points in Φ_y whose polar angle is greater than the reference point, and $\Phi_{r,y}$ is the set of points in Φ_y whose polar angle is smaller than the reference point. p_m and p_n are adjacent points in Φ_y. p_s is the reference point. The definition of λ is the same as formula (3-3).

As shown in Fig. 11, p_s is equal to T_3, which is blow the space plane. $\{\Pi\} = \{\Pi_1, \Pi_2, \Pi_3, \Pi_4\}$. i_1, i_2, i_3, i_4 are the intersection points of the space plane in $\{\Pi\}$ and the edge of $\Delta T_1T_2T_3$. $\Phi_1 = \{i_1, i_2, i_3, i_4\}$, $\Phi_2 = \{T_1, T_2\}$. The polar angle of T_1, i_1 and i_2 is greater than the polar angle of T_3. The polar angle of i_3, i_4 and T_2 is smaller than the polar angle of T_3 in the polar system with the observation point as the pole.

Case three: The observation point and the reference point are on the different sides of the dividing line, and the reference point is in the space plane. This case is computed as case two.

Case four: The observation point and the reference point are on the same side of the dividing line, and the reference point is above the space plane.

The area of the observed triangular surface that can be seen from the observation point can be calculated by the formula

$$S = S_{\Delta T_1T_2T_3} - \left|\sum_{p_m,p_n\in\Phi_{r,n}} \lambda_{p_m,p_n} S_{\Delta p_m p_n p_s}\right| - \left|\sum_{p_m,p_n\in\Phi_{l,n}} \lambda_{p_m,p_n} S_{\Delta p_m p_n p_s}\right| \quad (3-6)$$

where, $\Phi_n = \Phi_1 + \Phi_3$, the elements of Φ_n are deduplicated and arranged in descending order of polar angle. $\Phi_{l,n}$ is the set of points in Φ_n whose polar angle is greater than the polar angle of the reference point, and $\Phi_{r,n}$ is the set of points in Φ_n whose polar angle is smaller than the polar angle of the reference point. p_m and p_n are adjacent points in Φ_n. p_s is the reference point. The definition of λ is the same as formula (3-3). As is shown in Fig. 12, $p_s = T_3$, T_3 is above the space plane. $\{\Pi\} = \{\Pi_1, \Pi_2\}$. i_1, i_2, i_3, i_4 are the intersection points of the space plane in $\{\Pi\}$ and the edges of $\Delta T_1T_2T_3$. $\{\Phi_1 = i_1, i_2, i_3, i_4\}$, $\Phi_3 = \{T_1, T_2\}$. The polar angle of T_1, i_1 and i_2 is larger than the polar angle of T_3. The polar angle of i_3, i_4 and T_2 is smaller than the polar angle of T_3 in the polar system with the observation point as the pole.

Case five: The observation point and the reference point are on the same side of the dividing line, and the reference point is below the space plane.

The area of the observed triangular surface that can be seen from the observation point is calculated by the formula

$$S = S_{\Delta T_1T_2T_3} - \left|\sum_{p_m,p_n\in\Phi_n} \lambda_{p_m,p_n} S_{\Delta p_m p_n p_s}\right| \quad (3-7)$$

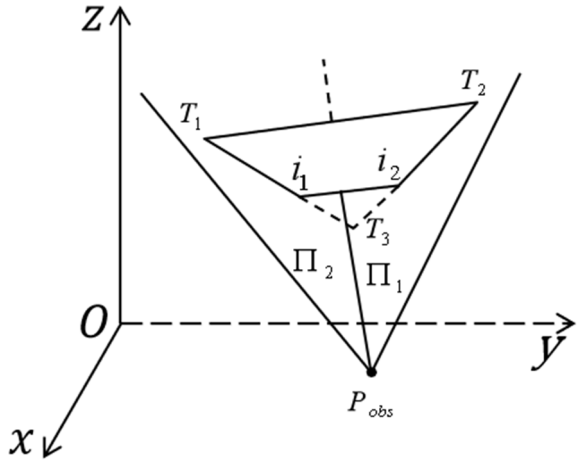

FIGURE 13. Model of spatial plane occluding triangular surface.

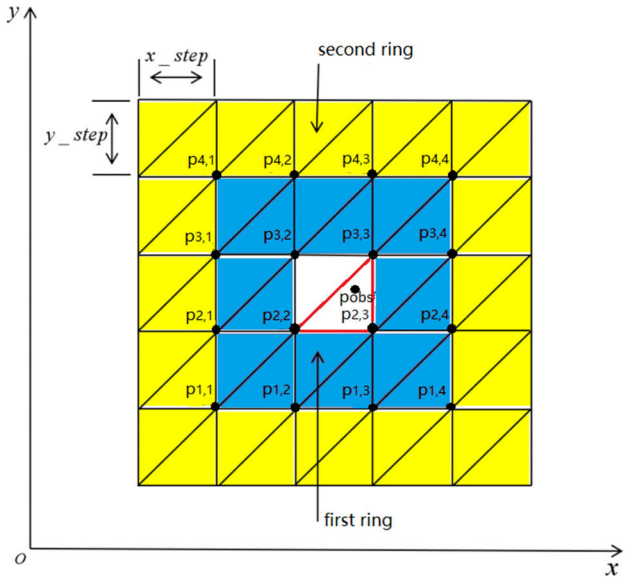

FIGURE 14. The top view of the terrain.

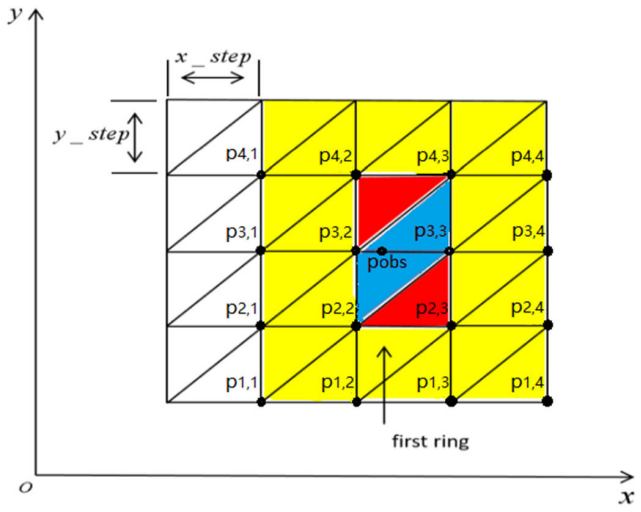

FIGURE 15. The observation point is on the right-angled side, excluding vertices of the triangular surface.

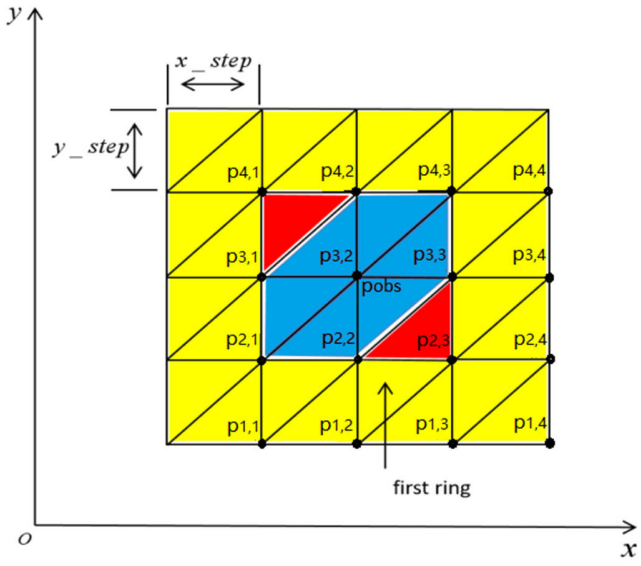

FIGURE 16. The observation point is vertex of the triangular surface.

where, $\Phi_n = \Phi_1 + \Phi_3$, the elements of Φ_n are deduplicated and arranged in descending polar order. p_m and p_n are adjacent points in Φ_n, p_s is the reference point. The definition of λ is the same as formula (3-3).

As is shown in Fig. 13, p_s is T_3, which is blow the space plane. $\{\Pi\} = \{\Pi_1, \Pi_2\}$. i_1, i_2 are the intersection points of the space plane in $\{\Pi\}$ and the edge of $\Delta T_1 T_2 T_3$. $\Phi_1 = \{i_1, i_2\}$, $\Phi_3 = \Phi$.

Case six: The observation point and the reference point are on the same side of the dividing line, and the reference point is in the space plane. This case is computed as case four.

D. CALCULATION OF THE SET OF THE VISIBLE SURFACES

Fig. 14 is the top view of the regular terrain. The coordinate of each point is (x, y, z). The index of each point is (i, j), where i is the row index, j is the column index, all starting from 0. *x_step* is the length of the cell in the x direction, and *y_step* is the length of the cell in the y direction.

The normal vector of the observation plane is $\overrightarrow{n_{obs}}$. Any point of the observation plane is p_i. The normal vector of the observed triangular surface is $\overrightarrow{n_{b\_c}}$. Any point of the observed triangular surface is p_j. If the observed triangular surface can be seen from the observation point, there is at least one pair of combinational (p_i, p_j) that satisfies the formula.

$$\begin{cases} \theta < \overrightarrow{p_i p_j}, \overrightarrow{n_{obs}} > \in [0, \dfrac{\pi}{2}) \\ \theta < \overrightarrow{p_j p_i}, \overrightarrow{n_{b\_c}} > \in [0, \dfrac{\pi}{2}) \end{cases} \quad (3-8)$$

There is at least one point p_i on the observation plane and one point p_j on the observed triangular surface. The angle between the vector $\overrightarrow{p_i p_j}$ and the normal vector of the observed triangular surface and the angle between the vector $\overrightarrow{p_j p_i}$ and the normal vector of the observation plane are all within the interval $[0, \pi/2)$.

Steps for calculating the set of visible triangular surfaces are as follows:

(1) Initialize the observation point and corresponding dictionary map_{obs}. Then process triangular surfaces within the smallest rectangle that contains the observation point and judge whether the triangular surface is visible through the formula (3-8). The area of the visible part of the triangular surface will be calculated if it is visible. The dictionary of observation point map_{obs} is updated with the observed triangular surface.

(2) Calculate the area of the triangular surface that can be seen from the observation point by the ring. As shown in Fig. 14, the blue region is the ring region closest to the observation point, which is called the first ring. In the ring, the area formed by the four adjacent vertices $p_{i,j}, p_{i+1,j}, p_{i,j+1}$, $p_{i+1,j+1}$ is the minimum processing unit. $p_{i,j}$, $p_{i+1,j}$, $p_{i,j+1}$, $p_{i+1,j+1}$ can be divided by two triangular surfaces. The triangular surface close to the observation point is first processed, and then the triangular surface far from the observation point is processed. If they are equidistant from the observation point, they can be processed in any order. After processing all the triangular surfaces in the ring, the dictionary of observation point map_{obs} will be updated with the triangular surfaces in the ring.

(3) After all the ring regions are processed the order of their distance from the observation point, the triangular surfaces visible from the observation point and the corresponding visible area are obtained.

The first step of calculating the set of visible triangular surfaces will change when the observation point is in different positions. If the observation point is inside the triangular element excluding the boundary, it is necessary to initialize the dictionary with the surface of the observation point and the polar angle interval of the surface, and calculate the visible area of the triangular surface adjacent to the hypotenuse of the triangular surface at the observation point. As shown in Fig. 14, the observation point is inside $\Delta p_{2,2}p_{2,3}p_{3,3}$ excluding the boundary. $map_{obs} = \{[0, 2\pi)$: $\Pi_{init}\}$, and Π_{init} is formed by $p_{2,2}, p_{2,3}, p_{3,3}$. Then the visible area of $\Delta p_{2,2}p_{3,3}p_{3,2}$ is calculated. As shown in Fig. 14, if the observation point is on hypotenuse $p_{2,2}$, $p_{3,3}$ of triangular surface excluding the vertices of triangular surface, $map_{obs} = \{I_1$: Π_1, I_2: Π_2. In this equation, I_1 is the polar interval of $\Delta p_{2,2}p_{2,3}p_{3,3}$, I_2 is the polar interval of $\Delta p_{2,2}p_{3,3}p_{3,2}$, Π_1 is the plane of $\Delta p_{2,2}p_{2,3}p_{3,3}$ and Π_2 is that of $\Delta p_{2,2}p_{3,3}p_{3,2}$. As shown in Fig. 15, if the observation point is on the right-angled side excluding vertices of the triangular surface, the observation point is on line segment $p_{3,2}p_{3,3}$ excluding vertices $p_{3,2}$ and $p_{3,3}$, $map_{obs} = \{I_1$: Π_1, I_2: $\Pi_2\}$. In this equation, I_1 is the polar interval of $\Delta p_{2,2}p_{3,3}p_{3,2}$, I_2 is the polar interval of $\Delta p_{3,2}p_{3,3}p_{4,3}$, Π_1 is the plane of $\Delta_{2,2}p_{3,3}p_{3,2}$ and Π_2 is that of $\Delta p_{3,2}p_{3,3}p_{4,3}$. Then the visible area of triangular surface in the red region is calculated. If the observation point is vertex of triangular surface, as shown in Fig. 16, it is necessary to initialize the dictionary with the polar angle interval of the triangular element in the blue region and the corresponding plane and calculate the visible area of the triangular surface in red region.

The update rule of the dictionary is to take the plane located above the space within the same polar angle. In one ring, the area formed by the four adjacent vertices $p_{i,j}$, $p_{i+1,j}$, $p_{i,j+1}$, $p_{i+1,j+1}$ is the minimum processing unit. $p_{i,j}$, $p_{i+1,j}$, $p_{i,j+1}, p_{i+1,j+1}$ can be divided by two triangular surfaces. The processes of calculating the area visible from the observation point are as follows:

(1) In the polar system with the observation point as the pole, $p_{i,j}$, $p_{i+1,j}$, $p_{i,j+1}$, and $p_{i+1,j+1}$ form a polar angle interval I_{four}. Then find the dictionary map_1 corresponding to I_{four} in map_{obs}.

(2) Among $p_{i,j}$, $p_{i+1,j}$, $p_{i,j+1}$, $p_{i+1,j+1}$, the point closest to the observation point is denoted as $p_{closest}$, and the point adjacent to the hypotenuse of $p_{closest}$ is denoted as p_a. If p_a is a point outside the current ring and does not belong to any of $p_{i,j}, p_{i+1,j}, p_{i,j+1}, p_{i+1,j+1}$, we will consider its impact on the calculation of the visible area, otherwise it will not be considered. As shown in Fig. 14, the blue area which is denoted as R is the first ring closest to the observation point. $p_{4,1}$ is the point of the outer circle of R, and $p_{3,2}$ is the point of the inner circle of R. In the polar system with the observation point as the pole, the polar angle interval formed by p_a and $p_{closest}$ is $I_{papclosest}$. If there is an intersection between $I_{papclosest}$ and I_{four}, we will consider its impact on the calculation of the visible area is necessary, otherwise the impact will not be considered. Then we discuss the case where $I_{papclosest}$ and I_{four} have the intersection. In the three-dimensional space, the plane $\Pi_{papclosest}$ is formed by $p_a, p_{closest}$ and the observation point. $I_{papclosest}$ and $\Pi_{papclosest}$ form the dictionary map_2, where $map_2 = \{I_{papclosest}$: $\Pi_{papclosest}\}$. Using map_2 to update map_1. If there are two vertices closest to the observation point, they are both need to be considered. As shown in Fig. 14, the plane formed by $p_{2,1}$, $p_{3,2}$, and p_{obs} and the plane formed by $p_{4,3}, p_{3,2}$ and p_{obs} will affect the calculation of the visible area of the triangular surfaces formed by the points $p_{3,1}, p_{4,1}, p_{3,2}$ and $p_{4,2}$, which are visible from the observation point.

(3) $p_{i,j}$, $p_{i+1,j}$, $p_{i,j+1}$, and $p_{i+1,j+1}$ can form two triangular surfaces A and B. First calculating the area of the triangular surface A that is close to the observation point with map_1. Then updating map_1 with triangular surface A, and calculating the area of triangular surface B with map_1.

IV. PROBABILITY-BASED POWER PROPAGATION MODEL

In order to study the influence of terrain simplification on predicting complex electromagnetic environment, a probability-based power propagation model is proposed. The triangular surfaces of the terrain fitted by the digital elevation model are mirror-smooth. Since the surface of terrain is rough and the terrain is composed of infinite number of micro-surfaces, the directions of micro-surfaces are random, and they are not always the same as that of macro triangular surface. Therefore, the process of power arrives at the ground from the transmitter is a deterministic event, which is transmitted between surfaces and finally reaches the receiving terminal as a probability-based event.

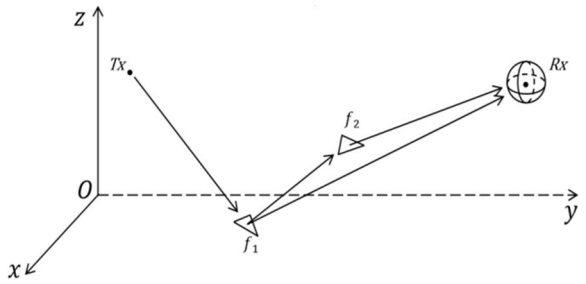

FIGURE 17. The probability-based propagation model with at most two reflections.

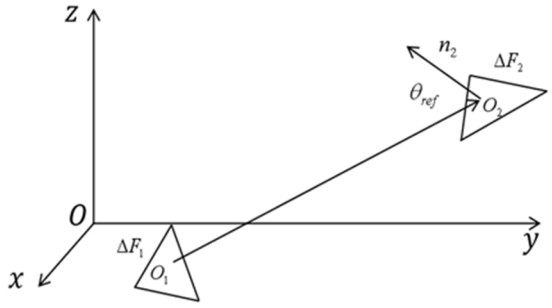

FIGURE 18. Power propagates from one triangular surface to the next.

In Fig. 17, the transmitter is represented by Tx, and the receiver is Rx. The visible triangular surface of Tx is f_1. The visible object of f_1 is f_2 and Rx. The visible object of f_2 is Rx. A certain probability of power is radiated from Tx to Rx through f_1 and f_2. A certain probability of power is radiated from Tx to Rx through f_1.

In Fig. 18, the power is transferred from triangular surface ΔF_1 to its visible triangular surface ΔF_2. The distance between the two visible triangular surfaces is

$$d_{O_1O_2} = \|O_1O_2\| \tag{4-1}$$

where, O_1 and O_2 are the gravity of surfaces ΔF_1 and ΔF_2, respectively.

The reflection angle [28], [29] is

$$\theta_{ref} = cos^{-1}\left(\frac{\overrightarrow{O_2O_1} \cdot \overrightarrow{n_2}}{|\overrightarrow{O_2O_1}|\|\overrightarrow{n_2}\|}\right) \tag{4-2}$$

where, $\overrightarrow{n_2}$ is the normal vector of micro-surface in ΔF_2, and $\overrightarrow{O_2O_1}$ is the vector from O_2 to O_1. As shown in Fig. 18, the reflection angle is between the vector $\overrightarrow{O_2O_1}$ and the normal vector of the triangular surface ΔF_2, and the reflection angle is defined on the triangular surface ΔF_2.

The solid angle [30]–[32] of the area visible to the triangular surface $\Delta F2$ seen from the triangular surface ΔF_1 with O_1 as the centre of sphere is

$$\Omega_{O_1O_2} = \frac{S_{\Delta F2,y}}{S_{\Delta F2}} \iint_{\Delta F_2} \frac{\overrightarrow{R} \cdot \overrightarrow{dS}}{\|\overrightarrow{R}\|^3} \tag{4-3}$$

where, $\overrightarrow{R}$ is the vector from O_1 to the any point on ΔF_2, and $S_{\Delta F2,y}$ is the area when ΔF_2 can be seen from O_1 the gravity of surfaces ΔF_1, $S_{\Delta F2}$ is the area of ΔF_2. The solid angle is

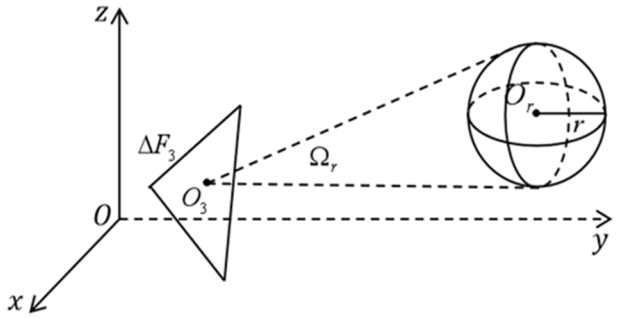

FIGURE 19. The solid angle of a sphere with r as its radius.

an area on the unit sphere. Therefore, the solid angle of the center of the sphere is equal to 4π for a unit sphere.

As shown in Fig. 19, the gravity of the triangular surface ΔF_3 is O_3, the center of the sphere is O_r, and the solid angle of the sphere of radius r relative to the point O_3 is

$$\Omega_{O_3O_r} = 2\pi\left[1 - \cos(tan^{-1}(\frac{r}{d_{\Omega_{O_3O_r}}}))\right] \tag{4-4}$$

The proportion of power radiated from the transmitter to the triangular surface is

$$u_{Tx,f} = \frac{\Omega_{\mathrm{Tx,f}}}{4\pi} \tag{4-5}$$

In the formula, $\Omega_{\mathrm{Tx,f}}$ is the solid angle of the visible surface of the transmitter on the unit ball with the transmitter position as the center of the sphere. It is the proportion of power radiated from the transmitter to the triangular surface. The rays are emitted in all directions by the transmitter, and is not blocked by terrain. Therefore, the denominator of the formula is 4π. The probability of power transferring from one triangular surface to the next is

$$u_{f,f} = \frac{\Omega_{\mathrm{f,f}}}{2\pi} \tag{4-6}$$

In the formula, $\Omega_{\mathrm{f,f}}$ is the solid angle of the triangular surface on the unit sphere with the gravity of the surface where the power is radiated as the center of sphere. The probability of power transfer from one triangular surface to the receiving sphere is

$$u_{f,Rx} = \frac{\Omega_{\mathrm{f},Rx}}{2\pi} \tag{4-7}$$

where, $\Omega_{\mathrm{f},Rx}$ is the solid angle of the receiving end on the unit ball whose center is the gravity of the surface where the power is radiated.

Formulas (4-6) and (4-7) show that the ray is transmitted from the triangular surface to the next triangular surface and the ray is transmitted from the triangular surface to the receiving ball. Since the ray can only be reflected from above the terrain surface rather than emitted in all directions like the transmitting ball, the denominator of the formula is 2π. The upper half unit ball divided by the terrain surface.

The power is transmitted from one surface through reflection, and the probability of one of the paths received by the

receiver through N − 1 reflection is

$$p_{f,Rx} = u_{f,Rx} \prod_{i=1}^{N-1} u_{f,f}^{i} \qquad (4-8)$$

The power is radiated from the transmitter, and the probability of one of the paths received by the receiver after N reflections is

$$p_{Tx,Rx} = u_{Tx,f} u_{f,Rx} \prod_{i=1}^{N-1} u_{f,f}^{i} = u_{Tx,f} p_{f,Rx} \qquad (4-9)$$

The power radiated by the transmitter and eventually received by the receiver after being reflected for N times is

$$P_{pow\_Rx} = P_{pow} \left(\frac{\lambda}{4\pi}\right)^2 \sum_{i=1}^{M} P_{Tx,Rx}^{N_i} \frac{\left|\sqrt{g_i} R_i^{N_i}\right|^2}{d_i^2} \qquad (4-10)$$

where, M is the number of effective channels through which the power transmitted by the transmitter is received by the receiver through the surfaces; P_{pow} is the transmitter power; g_i is the product of the transmit and receive antenna gain; N_i is the reflection number of the ith channel; d_i is the path length of the ith path; $R_i^{N_i}$ is the product of the reflection coefficient; P_{pow_Rx} is the power of the receiver; λ is the wavelength.

In the prediction of complex electromagnetic environment based on ray-tracing technology, the terrain simplification may change the path that is used between receiver and transmitter, accordingly affect the calculation results. The change of power of the receiver caused by the terrain simplification with the probability-based power propagation model is

$$\Delta P = P_{pow\_Rx'} - P_{pow\_Rx} \qquad (4-11)$$

where, P_{pow_Rx} is the power received by the receiver in the original terrain. $P_{pow\_Rx'}$ is the power received by the receiver when the terrain is simplified.

V. RESULTS AND ANALYSES

A. RESULT AND ANALYSIS ON ACCELERATION OF RADIO WAVE PROPAGATION PREDICTION BY TERRAIN SIMPLIFICATION

In order to study the radio wave propagation prediction time acceleration and result accuracy using the simplified terrain relative to the original terrain, this paper merely changes the threshold of terrain in the simulation, and other settings remain the same. The original accuracy of the terrain is 12m, and the width and the length of the terrain are both 4320m. The whole terrain consists of 260642 terrain triangles. And the whole terrain scene includes flat terrain and complex rugged terrain. The relative permittivity of the material is 25 and the electrical conductivity is 0.02S/m. The power of each transmitting antenna is 46dBm and the frequency of each transmitting antenna is 1000MHz. It is located in a relatively flat area. The height of the receiving antenna in the simulation is 10m, and the height of transmitting antenna is 30m, 40m and 50m, respectively. The transmitting antennas are located

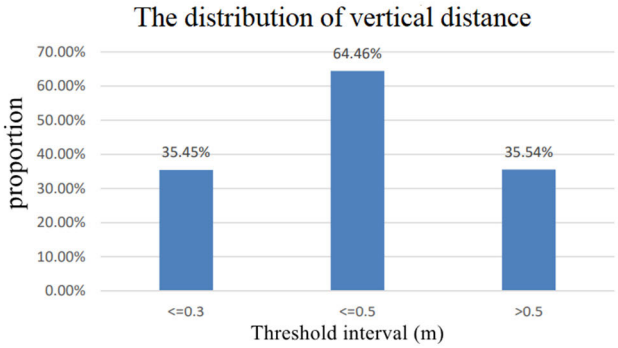

FIGURE 20. The distribution of vertical distance.

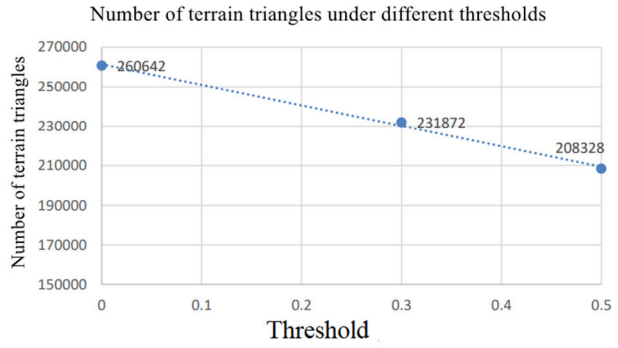

FIGURE 21. Number of terrain triangles under different thresholds.

in half way up the mountain. The simulation software is Wireless InSite.

The terrain simplification method can retain the basic framework of terrain to the greatest extent, and construct flat and rugged terrain with triangles with different accuracy, which can reduce the number of triangles required to construct terrain model and represent the multi-precision terrain. In this paper, the vertical distance distribution is used as a reference for threshold selection. As shown in Fig. 20, the number of vertical distances that is less than or equal to 0.3 accounts for 35.45% of the total vertical distance, the number of vertical distances that is less than or equal to 0.5 accounts for 64.46% of the total vertical distance, and the number of vertical distances that is greater than 0.5 accounts for 35.54% of the total vertical distance. Therefore, 0.3 and 0.5 are selected as the simplified threshold of the terrain. A terrain block is simplified, the number of triangular surfaces of the terrain block will be changed from 8 to 2, and the number of triangular surfaces is reduced by 6. The proportion of vertical distance increases by 35.45% from the original accuracy terrain to the terrain with threshold value of 0.3. The proportion of vertical distance increased by 29.01% from the threshold value of 0.3 to the threshold value of 0.5. The increment of the vertical distance from the original terrain to the threshold of 0.3 is greater than that from 0.3 to 0.5.

The simulation time in Fig. 22 includes the time to simplify the terrain. With the increase of threshold, the number of triangular surfaces is reduced and the simulation time is shortened. In the radio wave propagation prediction based on ray-tracing technology, the most time-consuming

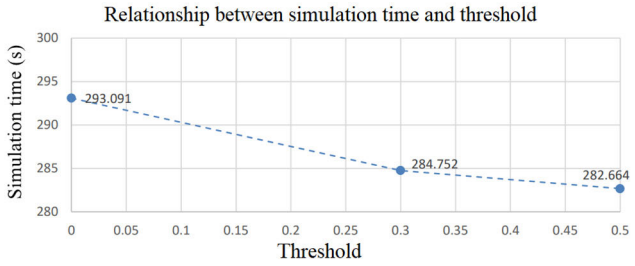

FIGURE 22. Relationship between simulation time and threshold.

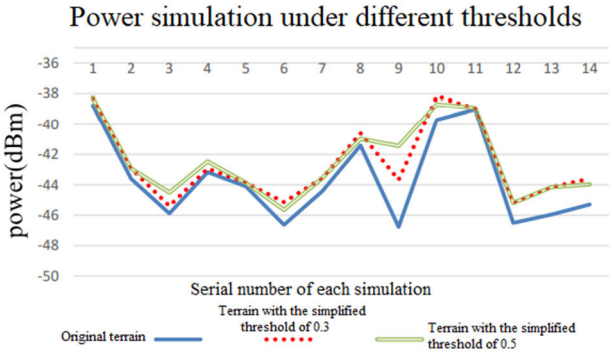

FIGURE 23. Power simulations under different thresholds.

part is calculating the intersection of ray and triangular surfaces. The tree structure is used to organize and store the data structure of triangular surfaces, and the time complexity is logarithmic with the number of triangular surfaces. As shown in Fig. 21 to Fig. 22, the reduction of simulation time is related to the reduction of the number of triangular surfaces.

To analyze the power error between using the simplified terrain and using the original terrain, power simulation under different terrain simplified thresholds is carried out in this paper. Fourteen simulations are carried out under each threshold. One receiver and one transmitter are set for each simulation. Only the coordinates and height of the transmitter and the coordinates of the receiver are changed for each simulation. In Fig. 23, the ordinate is the power received by the transmitter and the power unit is dBm. The abscissa is the serial number of each simulation. The solid blue line represents the simulated power under the original terrain. The red dotted line represents the simulated power under the terrain with the simplified threshold of 0.3; The green double solid line represents the simulated power under the terrain with the simplified threshold of 0.5. When the threshold is 0.3 and 0.5, the average error of power is 1.05dB and 1.19 dB, respectively. The formula of power error between using the simplified terrain and using the original terrain is

$$err_0 = \frac{\sum_{i=1}^{N} \left| P_i^j - P_0^j \right|}{n} \qquad (5-1)$$

In this formula, P_i^j is the power received by the receiver on the terrain simplified by threshold j in ith simulation. P_0^j is the power received by the receiver on the original terrain in ith simulation. n is the number of simulations.

TABLE 1. Simulation time reduction ratio and power deviation comparison under different thresholds.

THRESHOLD	Simulation time reduction ratio N_T(%)	Power deviation comparison err_0(dB)
0.3	2.85	1.05
0.5	3.56	1.19

The calculation formula of N_T in TABLE 1 is

$$N_T = \frac{T_0 - T_i}{T_0} \times 100\% \qquad (5-2)$$

In this formula, T_0 is the simulation time under the original terrain, T_i is the simulation time under the simplified terrain with the threshold i.

$$\mathrm{E} = \frac{err_0}{N_T} \qquad (5-3)$$

E is the power deviation when the unit simulation time is shortened, which is used as the indicator for the selection of terrain simplified threshold. When the terrain simplification threshold is 0.3, E is 0.3684. When the terrain simplified threshold is 0.5, E is 0.3343. By comparing E under different thresholds, when the threshold is 0.5, the value of E is the smallest, that is, the shortening of simulation time has the least impact on the power prediction results. Therefore, this threshold is used as the threshold of the terrain simplification. From the above analysis, it can be seen that within a certain allowable power error range, compared with the original terrain, simplifying the terrain can shorten the simulation time. For the terrain with large size and high modeling accuracy, terrain simplification has an obvious impact on the simulation time. And the main reason for power error is that the effective ray paths in the original terrain are different between those in the simplified terrain.

B. RESULT AND ANALYSIS OF THE IMPACT OF TERRAIN SIMPLIFICATION ON COMPLEX ELECTROMAGNETIC ENVIRONMENT BY THE PROBABILITY-BASED POWER MODEL

The simulation result of the probability-based power propagation model is compared with the simulation result of Wireless InSite to verify the accuracy of the probability-based power model. The original accuracy of the terrain is 12m, the width is 1008m and the length is 1008m. The whole terrain consists of 14112 terrain triangles. And the whole terrain scene includes flat terrain and complex rugged terrain. The relative permittivity of the material is 25 and the electrical conductivity is 0.02S/m. The power for each transmitting antenna is 46dBm and the frequency of each transmitting antenna is 1000MHz, and it is located in a relatively flat area. The height of the receiving antenna in the simulation is 10m and the height of transmitting antenna is 30m, 40m and 50m. All the transmitting antennas are located in half way up the mountain.

As shown in Fig. 24 and Table 2, the vertical distance less than or equal to 0.3 accounts for 45.39% of the total

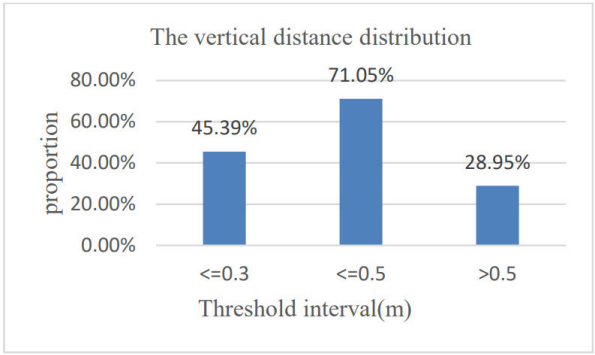

FIGURE 24. The vertical distance distribution of terrain.

TABLE 2. Units for magnetic properties.

Threshold	Number of triangular surfaces
0	14112
0.3,	11958
0.5	10740

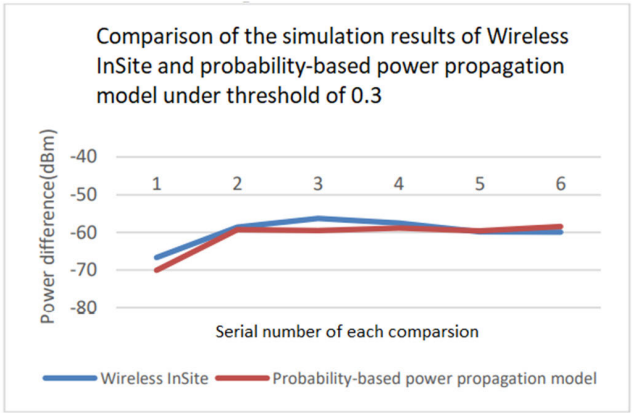

FIGURE 25. Comparison of the simulation results of Wireless InSite and probability-based power propagation model under threshold of 0.3.

vertical distance. In comparison with the original terrain, the number of triangular surfaces decreases by 15.26%. The vertical distance less than or equal to 0.5 accounts for 71.05% of the total vertical distance, and the number of triangular surfaces decreases by 23.89%. The percentage of vertical distance greater than 0.5 is extremely small. The simplification of terrain should retain the basic skeleton of the terrain in the radio wave propagation prediction model based on ray-tracing, and the terrain should not undergo drastic changes. Therefore, the thresholds for simplified terrain are 0.3 and 0.5.

To verify the accuracy of the probability-based power propagation model, comparisons of the simulation results of Wireless InSite and the model under different thresholds are carried out in this paper. At each threshold, the simulation results of Wireless InSite are compared with the model six times. One transmitter and one receiver are set for each simulation, and the coordinates and height of the transmitter are changed for each comparison. In Fig. 25 and Fig. 26,

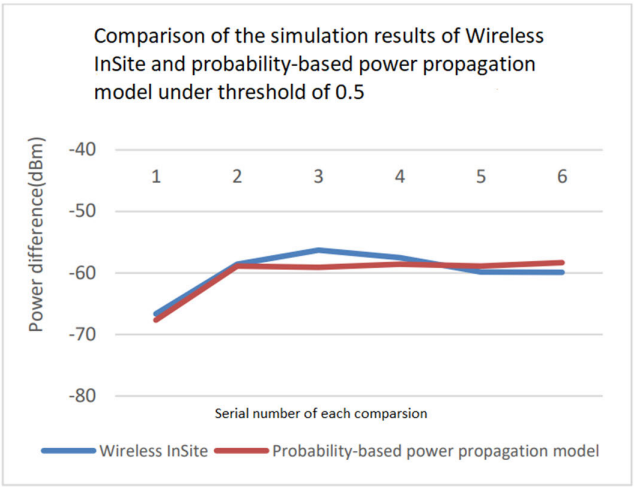

FIGURE 26. Comparison of the simulation results of Wireless InSite and probability-based power propagation model under threshold of 0.5.

the ordinate is comparison of the simulation results of Wireless InSite and the model under different thresholds. And the abscissa is the serial number of each comparison. The blue curve and the red curve represent the power difference between power obtained under the original terrain and the power obtained after the terrain is simplified under the thresholds. The calculation method of ordinate "power difference" is shown in formula (5-4).

$$\Delta \mathrm{P} = P'_{\mathrm{pow\_Rx}} - P_{\mathrm{pow\_Rx}} \tag{5-4}$$

$P_{\mathrm{pow\_Rx}}$ is the power received by the receiver in the original terrain; $P'_{\mathrm{pow\_Rx}}$ is the power received by the receiver after the terrain is simplified. Since the ordinate is the power difference rather than the power value, the results in Fig. 21 and 22 are always negative values.

The minimum error between the simulation result of the probability-based power propagation model and the WI simulation result is 0.5018dB. The average error is 1.5039dB. It can be verified that the probability-based power propagation model can better analyze the influence of terrain simplification on the receiver power. The formula of error between the simulation results of the probability-based propagation model and the simulation results of WI is

$$\mathrm{error} = \frac{\sum_1^2 |\Delta Pp - \Delta Pw|}{2} \tag{5-5}$$

The unit is dB, ΔPp is the difference between the power of receiver under a given threshold and that in the original terrain predicted with the probability-based power propagation model. ΔPw is the difference between the power of receiver obtained by WI simulation and that in the original terrain under a given threshold.

VI. CONCLUSION

As for the simplification of terrain, the numerical matrix of the original terrain is divided into 3 × 3 blocks. The results of Douglas–Peucker algorithm in four directions of row, column, positive and negative diagonal are considered compre-

TABLE 3. Symbol map.

Symbol	SECTION	Definition
p_{obs}	III.A	the observation point
$\overrightarrow{n_{b\_c}}$	III.A	the normal vector of the observed triangular surface
map_{obs}	III.B	the dictionary of the observation point p_{obs}
$\{\Pi\}$	III.B	the set of all space planes in map_{obs} containing the polar angle range of the observed triangular plane
Φ_{inner}	III.B	The set of points formed by the intersection of the two adjacent space planes in $\{\Pi\}$ and the plane of the observed triangular surface inside the observed triangular surface
Φ_{bd}	III.B	The set of points formed by the intersection of the two adjacent space plane in $\{\Pi\}$ and the edges of the observed triangular surface
Φ_1	III.B	addition of set Φ_{inner} and set Φ_{bd}
Φ_2	III.B	the set of visible vertices in the observed triangular surface
Φ_3	III.B	the set of invisible vertices in the observed triangular surface
Φ_y	III.C	addition of set Φ_1 and set Φ_2
$\Phi_{l,y}$	III.C	the set of points in Φ_y whose polar angle is greater than the reference point
$\Phi r,y$	III.C	the set of points in Φ_y whose polar angle is smaller than the reference point
Φ_n	III.C	addition of set Φ_1 and set Φ_3
$\Phi_{l,n}$	III.C	the set of points in Φ_n whose polar angle is greater than the polar angle of the reference point
$\Phi_{r,n}$	III.C	the set of points in Φ_n whose polar angle is smaller than the polar angle of the calculation starting point
$\overrightarrow{n_{b\_c}}$	III.D	the normal vector of the observed triangular surface
$\overrightarrow{n_{obs}}$	III.D	the normal vector of the observation plane
I_{four}	III.D	a polar angle interval formed by four adjacent vertices $p_{i,j}$, $p_{i+1,j}$, $p_{i,j+1}$, $p_{i+1,j+1}$
$p_{closest}$	III.D	the point closest to the observation point among $p_{i,j}$, $p_{i+1,j}$, $p_{i,j+1}$, $p_{i+1,j+1}$
p_a	III.D	the point adjacent to the hypotenuse of $p_{closest}$ among $p_{i,j}$, $p_{i+1,j}$ $p_{i,j+1}$, $p_{i+1,j+1}$
$I_{papclosest}$	III.D	the polar angle interval formed by p_a and $p_{closest}$
$\Pi_{papclosest}$	III.D	the plane formed by p_a, $p_{closest}$ and the observation point
Tx	IV	transmitter
Rx	IV	receiver
$d_{O_1O_2}$	IV	the distance between the two visible triangular surfaces
θ_{ref}	IV	the reflection angle is between the vector $\overrightarrow{O_2O_1}$ and the normal vector of the triangular surface ΔF_2
$\Omega_{O_1O_2}$	IV	The solid angle of the area visible to the triangular surface ΔF_2 seen from the triangular surface ΔF_1 with O_1 as the centre of sphere
$\Omega_{O_3O_r}$	IV	the solid angle of the sphere of radius r relative to the point O_3
$u_{Tx,f}$	IV	the proportion of power radiated from the transmitter to the triangular surface
$u_{f,f}$	IV	the probability of power transferring from one triangular surface to the next
$u_{f,Rx}$	IV	the probability of power transfer from one triangular surface to the receiving sphere
$p_{f,Rx}$	IV	the probability of one path, on which the power is transmitted from a surface and then received by the receiving end after being reflected for N times
$p_{Tx,Rx}$	IV	the probability of one path, on which the power is transmitted from the transmitter and then received by the receiver after being reflected for N times
P_{pow_Rx}	IV	the power radiated by the transmitter and finally received by the receiver after being reflected for N times
ΔP	IV	the change of power of the receiver caused by the terrain simplification with the probability-based power propagation model

hensively in each small terrain, by which the shortcoming of neglecting the influence of adjacent nodes in a certain direction can be made up. The vertical distance distribution obtained in the pretreated terrain is used as a reasonable reference for the selection of the threshold of terrain simplification.

In order to analyze the influence of terrain simplification on the prediction accuracy of complex electromagnetic environment, two algorithms are proposed, which are the visibility algorithm based on the relationship between triangular plane and plane in space and the probability-based power propagation model. The areas of visible and visible surfaces are calculated with the visibility algorithm. In reality, the terrain is composed of a large number of micro-surfaces. Not all the normal vectors of micro-surfaces are the same as the macro normal vectors. Therefore, the process of power transfer from the transmitting source to the receiving end through the surfaces is regarded as a probabilistic process. The probability-based power propagation model uses the results of the visibility algorithm to calculate the probability of power propagation, and is combined with the characteristics of radio wave propagation to calculate the variation in the prediction results caused by terrain simplification.

APPENDIX

See Table 3.

REFERENCES

[1] Q. Zhou and Y. Chen, "Generalization of DEM for terrain analysis using a compound method," *ISPRS J. Photogramm. Remote Sens.*, vol. 66, no. 1, pp. 38–45, Jan. 2011.

[2] A. V. Kiselev, A. V. Nikulin, and V. V. Artyushenko, "The algorithm for calculating reflecting signal power characteristics based on terrain digital map," in *Proc. 18th Int. Conf. Young Spec. Micro/Nanotechnolog. Electron Devices (EDM)*, Jun. 2017, pp. 115–118.

[3] K. Rizk, J.-F. Wagen, and F. Gardiol, "Two-dimensional ray-tracing modeling for propagation prediction in microcellular environments," *IEEE Trans. Veh. Technol.*, vol. 46, no. 2, pp. 508–518, May 1997.

[4] P. Kreuzgruber, P. Unterberger, and R. Gahleitner, "A ray splitting model for indoor radio propagation associated with complex geometries," in *Proc. IEEE 43rd Veh. Technol. Conf.*, May 1993, pp. 227–230.

[5] J. W. McKown and R. L. Hamilton, "Ray tracing as a design tool for radio networks," *IEEE Netw.*, vol. 5, no. 6, pp. 27–30, Nov. 1991.

[6] S. Y. Seidel and T. S. Rappaport, "A ray-tracing technique to predict path loss and delay spread inside buildings," in *Proc. Conf. Rec. GLOBECOM Commun. Global Users*, vol. 2, Dec. 1992, pp. 649–653.
[7] R. Valenzuela, "A ray tracing approach to predicting indoor wireless transmission," in *Proc. IEEE 43rd Veh. Technol. Conf.*, May 1993, pp. 214–218.
[8] Y.-B. Tao, H. Lin, and H. J. Bao, "KD-tree based fast ray-tracing for RCS prediction," *Prog. Electromagn. Res.*, vol. 81, pp. 329–341, 2008.
[9] Y. Dong and G. Tang, "Comparison of popular methods for simplifying terrain based on grid DEMs," in *Proc. 2nd Conf. Environ. Sci. Inf. Appl. Technol.*, Jul. 2010, pp. 227–230.
[10] M. Lounsbery and T. DeRose, "Multiresolution analysis for surfaces of arbitrary topological type," *ACM Trans. Graph.*, vol. 16, pp. 34–73, Jan. 1994.
[11] M. Eck, T. DeRose, T. Duchamp, H. Hoppe, M. Lounsbery, and W. Stuetzle, "Multiresolution analysis of arbitrary meshes," in *Proc. 22nd Annu. Conf. Comput. Graph. Interact. Techn. (SIGGRAPH)*, 1995, pp. 173–182.
[12] W. Maocai, D. Guangming, D. Anhong, and L. Yan, "A study on data simplification of 3D terrain in using wavelets analysis," *Comput. Eng. Appl.*, vol. 51, pp. 47–48, Nov. 2003.
[13] H. Lanfang, "Modeling and simulation of mountainous terrain based on wavelet analysis," in *Proc. 9th Int. Conf. Measuring Technol. Mechatronics Autom. (ICMTMA)*, Jan. 2017, pp. 292–295.
[14] D. H. Douglas and T. K. Peucker, "Algorithms for the reduction of the number of points required to represent a digitized line or its caricature," *Cartographica, Int. J. Geographic Inf. Geovisualization*, vol. 10, no. 2, pp. 112–122, 1973.
[15] S.-T. Wu and M. R. G. Marquez, "A non-self-intersection Douglas–Peucker algorithm," in *Proc. 16th Brazilian Symp. Comput. Graph. Image Process. (SIBGRAPI)*, 2003, pp. 60–66.
[16] H. Jin and F. Lifan, "Three-dimensional Douglas–Peucker algorithm and the study on its application to automated generalization of DEM," *Proc. SPIE*, vol. 6420, Oct. 2006, Art. no. 64200M.
[17] H. Bin and L. Song, "A solution to polygonal blanking problem in 3-D space based on the improved painter algorithm," in *Proc. 2nd Int. Congr. Image Signal Process.*, Oct. 2009, pp. 1–4.
[18] Z. Ma and J. Ma, "Comparisons among some surface blanking approaches," *Sci. Technol. Inf.*, vol. 2, no. 2, pp. 69–71, Jan. 2008.
[19] C. Saeidi and F. Hodjatkashani, "Modified angular Z-buffer as an acceleration technique for ray tracing," *IEEE Trans. Antennas Propag.*, vol. 58, no. 5, pp. 1822–1825, May 2010.
[20] F. S. de Adana, O. G. Blanco, I. G. Diego, J. P. Arriaga, and M. F. Catedra, "Propagation model based on ray tracing for the design of personal communication systems in indoor environments," *IEEE Trans. Veh. Technol.*, vol. 49, no. 6, pp. 2105–2112, Nov. 2000.
[21] M. F. Catedra, J. Perez, F. S. de Adana, and O. Gutierrez, "Efficient ray-tracing techniques for three-dimensional analyses of propagation in mobile communications: Application to picocell and microcell scenarios," *IEEE Antennas Propag. Mag.*, vol. 40, no. 2, pp. 15–28, Apr. 1998.
[22] F. A. Agelet, A. Formella, J. M. H. Rabanos, F. I. D. Vicente, and F. P. Fontan, "Efficient ray-tracing acceleration techniques for radio propagation modeling," *IEEE Trans. Veh. Technol.*, vol. 49, no. 6, pp. 2089–2104, Nov. 2000.
[23] J. Maurer, O. Drumm, D. Didascalou, and W. Wiesbeck, "A novel approach in the determination of visible surfaces in 3D vector geometries for ray-optical wave propagation modelling," in *Proc. IEEE 51st Veh. Technol. Conf.*, May 2000, pp. 1651–1655.
[24] K. H. Ng, E. K. Tameh, A. Doufexi, M. Hunukumbure, and A. R. Nix, "Efficient multielement ray tracing with site-specific comparisons using measured MIMO channel data," *IEEE Trans. Veh. Technol.*, vol. 56, no. 3, pp. 1019–1032, May 2007.
[25] J. Bittner, P. Wonka, and M. Wimmer, "Visibility preprocessing for urban scenes using line space subdivision," in *Proc. Pacific Conf. Comput. Graph. Appl.*, Oct. 2001, pp. 276–284.
[26] R. P. Torres, L. Valle, M. Domingo, and S. Loredo, "An efficient ray-tracing method for radiopropagation based on the modified BSP algorithm," in *Proc. Gateway to 21st Century Commun. Village. VTC -Fall. IEEE VTS 50th Veh. Technol. Conf.*, Sep. 1999, pp. 1967–1971.
[27] S. Hussain and C. Brennan, "Efficient preprocessed ray tracing for 5G mobile transmitter scenarios in urban microcellular environments," *IEEE Trans. Antennas Propag.*, vol. 67, no. 5, pp. 3323–3333, May 2019.
[28] P. F. Daley and F. Hron, "Reflection and transmission coefficients for transversely isotropic media," *Bull. Seismolog. Soc. Amer.*, vol. 67, pp. 661–675, Jun. 1977.
[29] P. F. Daley and F. Hron, "Reflection and transmission coefficients for seismic waves in ellipsoidally anisotropic media," *Geophysics*, vol. 44, no. 1, pp. 27–38, Jan. 1979.
[30] R. P. Gardner and K. Verghese, "On the solid angle subtended by a circular disc," *Nucl. Instrum. Methods*, vol. 93, pp. 163–167,1971.
[31] H. Gotoh and H. Yagi, "Solid angle subtended by a rectangular slit," *Nucl. Instrum. Methods*, vol. 96, no. 3, pp. 485–486, Oct. 1971.
[32] P. Obložinsky and I. Ribanský, "The solid angle subtended at a disk source by a non-parallel disk detector," *Nucl. Instrum. Methods*, vol. 94, no. 1, pp. 187–188, Jun. 1971.

DAN SHI (Member, IEEE) received the Ph.D. degree in electronic engineering from the Beijing University of Posts and Telecommunications, Beijing, China, in 2008.

She is currently a Professor with the Beijing University of Posts and Telecommunications. She has published more than 100 papers in academic journals and conferences at home and abroad. Her research interests include electromagnetic compatibility, ultra-wideband wireless communication, and mobile internet. She is the Chair of the IEEE EMC Beijing Chapter, the Vice Chair of URSIE Commission in China, and the Secretary General of EMC Section of China Institute of Electronics.

ZHEN ZHANG received the master's degree from the Beijing University of Posts and Telecommunications, Beijing, China, in 2021.

His current research interests include electromagnetic compatibility, ultra-wideband wireless communication, and mobile internet.

FENGSHUO WEI is currently pursuing the master's degree with the Beijing University of Posts and Telecommunications, Beijing, China. His current research interests include electromagnetic compatibility, ultra-wideband wireless communication, and mobile internet.

CHENG LIAN received the bachelor's degree in electronic engineering from the Chongqing University of Posts and Telecommunications, Chongqing, China, in 2020. He is currently pursuing the master's degree in electronic engineering with the Beijing University of Posts and Telecommunications, Beijing, China. His research interests include electromagnetic compatibility and machine learning.